Computers, Materials & Continua

Tech Science Press

https://doi.org/10.32604/cmc.2026.083976

ARTICLE

Structural Damage Diagnosis Based on Multi-Stage Sparrow Search Algorithm

Lijun Yang[1] and Qiuwei Yang[2,*]

[1]School of Civil Engineering, Shaoxing University, Shaoxing, China
[2]Zhejiang Key Laboratory of Intelligent Construction and Operation & Maintenance for Deep-Sea Foundations, Ningbo University of Technology, Ningbo, China

*Corresponding Author: Qiuwei Yang. Email: yangqiuwei79@gmail.com

Received: 14 April 2026; Accepted: 25 June 2026; Published: 23 July 2026

ABSTRACT: This study proposes a Multi-Stage Sparrow Search Algorithm (MS-SSA) for precise structural damage identification. Initially, the structural static displacement sensitivity formulation is derived via the Sherman-Morrison-Woodbury formula, and an objective function is constructed by integrating the sensitivity equations with the L2-norm penalty. Subsequently, MS-SSA is implemented to sequentially achieve preliminary damage localization and accurate quantification. In the localization phase, a constrained narrow-bound search space is predefined to identify potential damage regions. Leveraging this feedback, the sensitivity equations are condensed, and the search boundaries are adaptively refined for the quantification phase, where SSA is reapplied to precisely determine damage severity while mitigating misjudgments. The MS-SSA framework exhibits two distinct advantages: (i) Phase I localization accelerates convergence by constraining the search space, as it does not target precise quantification; and (ii) the significant reduction in unknowns achieved by excluding intact elements in Phase II enables rapid convergence to the global optimum. Comparative studies against the Grey Wolf Optimizer (GWO), Whale Optimization Algorithm (WOA), and standard SSA demonstrate that the proposed method effectively overcomes computational instability, slow convergence, and large errors inherent in swarm intelligence optimization for damage identification. Specifically, numerical case studies reveal that the identification error is reduced to merely 9%~22% of that associated with existing methods, with experimental validation confirming reductions to 18%~22%. Overall, the proposed approach achieves high-fidelity damage identification while eliminating false positives and false negatives.

KEYWORDS: Damage diagnosis; static displacement; sensitivity; Sparrow Search Algorithm (SSA); narrow search range

1 Introduction

Engineering structures inevitably deteriorate and sustain damage during their service life. Consequently, timely and accurate damage identification is paramount to ensuring structural safety and preventing catastrophic failures. Current damage diagnosis methodologies can be broadly classified into two categories: dynamic diagnostic methods and static diagnostic methods. Dynamic diagnostic methods [1,2] are well-suited for online structural health monitoring (SHM). For instance, Ruiz et al. [3] proposed a damage detection strategy for beam-like structures based on frequency response functions, training decision trees, support vector machines, and artificial neural networks for localization. Gandelli et al. [4] investigated the relationship between operational modal analysis and damage detection through tests on prestressed concrete beams. Feng et al. [5] introduced a novel method for detecting single and composite damage in offshore structures under soil-structure interaction, integrating wavelet transforms with a multi-scale depthwise convolutional neural network. Nouri et al. [6] utilized the Fourier decomposition method to identify damage in wooden bridges via vibration data. Teng et al. [7] developed an unsupervised damage detection framework employing an attention-based convolutional autoencoder to reconstruct real-time vibration signals. Lyu et al. [8] estimated modal parameters using a continuous scanning laser Doppler vibrometer system, while Mansouri et al. [9] optimized damage assessment in beams based on joint-induced vibrations, demonstrating that the Dynamic Beetle Optimization (DBO) algorithm yields superior localization accuracy. di Marzo et al. [10] revealed that introducing an additional mass near a damaged region amplifies the frequency shifts between undamaged and damaged states. Wang and Cha [11] conducted a comparative analysis of four machine learning and one deep learning method for detecting bolt-loosening in steel bridges. Peng et al. [12] constructed damage diagnosis equations using mode shape sensitivity, addressing limitations caused by insufficient measurement points and modal orders. Zar et al. [13] reviewed the evolution of vibration-based detection, highlighting the innovative capabilities of convolutional neural networks in raw data feature extraction. Despite these advancements, dynamic methods face persistent challenges [14]: (1) most algorithms assume non-damping and constant mass, compromising data accuracy; (2) capturing clear mode shapes for large-scale civil structures remains difficult; and (3) some stiffness-based methods often require hard-to-obtain high-order modal data.

In contrast, static diagnostic methods offer a promising alternative to overcome these limitations, as static responses are directly correlated with structural stiffness and are easier to measure accurately. Peng and Yang [15] proposed a static shear energy index for assessing beam damage. Abedin et al. [16] evaluated a 50-year-old precast-prestressed bridge through static and dynamic load tests, proposing a tailored SHM method. Cristiani et al. [17] utilized convolutional neural networks with distributed fiber-optic sensors to predict delamination in CFRP specimens. Al Thobiani et al. [18] combined the Extended Finite Element Method with the Grey Wolf Optimizer for crack identification, validating accuracy through static and modal analyses. Ge et al. [19] developed a vision-based system for displacement measurement and damage assessment of simply supported beams. Xiao et al. [20] introduced a stiffness separation technique for long-span truss bridges, establishing equilibrium equations for inverse analysis. Kardoulias et al. [21] trained neural networks on finite element data under static and dynamic loads to determine key SHM parameters. Fayyadh and Abdul Razak [22] found that static-based shear stiffness indices exhibit higher sensitivity to degradation than flexural indices or dynamic-based metrics. Naderpour et al. [23] employed image processing techniques to classify damage patterns in reinforced concrete beams and subsequently implemented Support Vector Machine and k-Nearest Neighbor algorithms to determine the damage type, location, and severity.

However, in practical engineering, the volume of available experimental data is often significantly smaller than the number of unknown structural parameters. This data scarcity poses substantial challenges for damage assessment in large-scale structures, frequently leading to misjudgment or omission. Metaheuristic algorithms [24] have emerged as a promising solution. These algorithms employ heuristic rules inspired by natural and social phenomena to navigate complex search spaces. As delineated by Cuevas and Rodríguez [24], key characteristics of metaheuristic algorithms include population-based search, stochastic behavior, and a balance between exploration and exploitation. Population-based search evolves a set of candidate solutions iteratively. Stochastic behavior guides the search direction via probabilistic processes. The balance between exploration (global searching) and exploitation (local refinement) determines the algorithm's efficacy. Popular metaheuristic algorithms include Genetic Algorithms (GA) [25], Particle Swarm Optimization (PSO) [26], Cuckoo Search (CSA) [27], Whale Optimization Algorithm (WOA) [28], Grey Wolf Optimizer (GWO) [29], Gravitational Search Algorithm (GSA) [30], and Differential Evolution (DEA) [31].

The Sparrow Search Algorithm (SSA), recently developed by Xue and Shen [32], simulates the foraging and anti-predation behaviors of sparrow populations, categorizing individuals into discoverers, followers, and scouts. Discoverers explore the search space, followers conduct local foraging, and scouts enable escape mechanisms, balancing global and local searches. Xue and Shen [32] verified SSA's superiority over GWO, PSO, and GSA in computational speed, stability, and convergence accuracy using 19 benchmark functions. Yan et al. [33] further confirmed SSA's advantages in convergence speed and precision. Review papers [34,35] highlight SSA's widespread application in machine learning, energy systems, and path planning. While some researchers [12,36,37] have applied SSA to vibration-based damage identification, the aforementioned limitations of dynamic methods persist. Therefore, integrating SSA with static damage diagnosis theory is highly necessary to develop high-precision, practical tools for engineering. This study pioneers the integration of SSA with static diagnosis theory. It aims to develop a robust methodology for accurate structural damage identification using limited static test data. The innovations are twofold. First, a numerical approach is proposed to calculate structural static displacement sensitivity based on the Sherman-Morrison-Woodbury (SMW) formula. This enables efficient computation for large-scale finite element models. A novel objective function is then constructed by integrating displacement sensitivity with the L2-norm penalty of the solution vector. Second, a customized Multi-Stage Sparrow Search Algorithm (MS-SSA) is developed. Phase I employs a constrained narrow-bound search space for preliminary localization. This accelerates convergence as it does not target precise quantification. Phase II leverages feedback from Phase I to condense the sensitivity equations and adaptively refine the search boundaries. By excluding intact elements, Phase II significantly reduces the number of unknowns. This enables rapid convergence to the global optimum for precise quantification. This framework effectively mitigates misjudgments. The reliability and superiority of MS-SSA are rigorously validated through a single numerical simulation and a single experimental case study.

The structure of this paper is organized as follows. Section 2 illustrates the fundamental principles, core formulas and implementation procedures of the methods proposed in this work. Section 3 presents the research results of one numerical example and one experimental case. Section 4 carries out an in-depth discussion on the results of the case studies. Section 5 draws the main conclusions of this study.

2 Methodology

This section systematically elaborates the methodological framework adopted in this study. First, the derivation of static displacement sensitivity via the SMW formula is presented. Subsequently, the mechanism for achieving preliminary damage localization using the SSA in the first stage is elucidated. Finally, the procedure for implementing SSA to perform precise damage quantification in the second stage is detailed.

2.1 Static Displacement Sensitivity

Static displacement serves as the most prevalent response parameter for structural damage detection. In engineering practice, static displacements can be readily measured using dial indicators, Linear Variable Differential Transformers (LVDTs), and optical measurement systems. A sensitivity formulation is established to characterize the relationship between structural damage parameters and variations in static displacement. In this study, a numerical approach for calculating static displacement sensitivity is proposed. For a structure with n degrees of freedom (DOFs), the static displacements under gravitational loading before and after damage occurrence are computed using the finite element model (FEM) via the following equations:

$$K_u d_u = l \tag{1}$$

$$K_d d_d = l \tag{2}$$

$$K_d = K_u - \Delta K \tag{3}$$

$$d_d = d_u + \Delta d \tag{4}$$

herein, K_u denotes the stiffness matrix of the intact structure, d_u represents the corresponding static displacement vector under the external load vector l. K_d denotes the stiffness matrix of the damaged structure, and d_d represents the corresponding displacement vector. Meanwhile, ΔK and Δd denote the changes in the stiffness matrix and displacement caused by structural damage, respectively. Based on the finite element method principle, the variation of the global stiffness matrix can be expressed as the sum of the product of each elemental stiffness matrix and the damage coefficient, i.e.,

$$\Delta K = \sum_{i=1}^{N} \alpha_i K_i, (\alpha_i \subset [0,1]) \tag{5}$$

where K_i and α_i denote the elemental stiffness matrix and the damage coefficient corresponding to the i-th element, respectively, while N represents the total number of elements in the structural FEM. To derive the displacement sensitivity with respect to the i-th element, the damage is localized exclusively to this specific element. Consequently, Eq. (5) is simplified as follows:

$$\Delta K = \alpha_i K_i \tag{6}$$

Substituting Eq. (6) into Eq. (3) yields:

$$K_d = K_u - \alpha_i K_i \tag{7}$$

Using Eqs. (1) and (2), the displacement vectors for the intact and damaged states are formulated as follows:

$$d_u = K_u^{-1} \cdot l \tag{8}$$

$$d_d = K_d^{-1} \cdot l \tag{9}$$

Leveraging Eq. (7), the inverse of the damaged structural stiffness matrix is efficiently computed via the SMW formula [38] as follows:

$$K_i = C_i C_i^T \tag{10}$$

$$K_d^{-1} = K_u^{-1} + \alpha_i K_u^{-1} C_i \left(I + \alpha_i C_i^T K_u^{-1} C_i\right)^{-1} C_i^T K_u^{-1} \tag{11}$$

In Eq. (10), C_i denotes a full-rank matrix with dimensions $n \times r$, obtained via the decomposition of K_i, where r represents the rank of K_i ($r \ll n$). This decomposition is implemented using spectral decomposition [39]. Subsequently, by combining Eqs. (4), (8), (9) and (11), the displacement difference vector between the intact and damaged states is derived as follows:

$$\Delta d = \alpha_i K_u^{-1} C_i \left(I + \alpha_i C_i^T K_u^{-1} C_i\right)^{-1} C_i^T K_u^{-1} l \tag{12}$$

From Eq. (12), the displacement sensitivity vector ξ_i corresponding to the i-th element can be calculated as:

$$\xi_i = \frac{\Delta d}{\alpha_i} = K_u^{-1} C_i \left(I + \alpha_i C_i^T K_u^{-1} C_i\right)^{-1} C_i^T K_u^{-1} l \tag{13}$$

For a linear structure exhibiting simultaneous multi-element damage, the expression for the displacement difference vector is formulated based on the principle of linear superposition as follows:

$$\Delta d = \sum_{i=1}^{N} \alpha_i \xi_i \tag{14}$$

Eq. (14) can be rewritten in matrix notation as:

$$A \cdot x = y \tag{15}$$

where

$$x = (\alpha_1, \alpha_2, \cdots, \alpha_N)^T \tag{16}$$

$$A = [\xi_1, \xi_2, \cdots, \xi_N] \tag{17}$$

$$y = \Delta d \tag{18}$$

In Eq. (15), A denotes the coefficient matrix, x represents the vector of unknown damage coefficients, and y corresponds to the vector of measured responses. It should be emphasized that the number of equations can be augmented by adjusting static loading patterns, thereby providing sufficient constraints to solve for α_i. Ideally, the system should be well-posed, maintaining a comparable number of equations and unknowns; this balance is practically achieved by introducing multiple independent static loading cases. Consequently, the unknown damage coefficients α_i can be determined using Eq. (15), forming the basis for evaluating the damage state of each element. Prevailing solution methodologies include the generalized inverse method, singular value truncation, and swarm intelligence optimization algorithms, such as GA, PSO, CSA, WOA, and GWO.

2.2 Damage Localization via Phase I SSA with Constrained Search Space

Xue and Shen [32] introduced the SSA, an innovative swarm intelligence optimizer inspired by the foraging behavior and anti-predation mechanisms of sparrow flocks. Within the SSA framework, the population is categorized into three distinct roles: producers, scroungers, and scouts. Producers spearhead the exploration of new food sources—corresponding to the discovery of promising candidate solutions in the search space. Individuals with superior fitness values are typically assigned this role to guide the population toward optimal regions. Scroungers emulate the foraging strategies of producers, leveraging acquired information to refine their positions and secure better solutions during iterations. scouts are tasked with environmental monitoring and risk assessment; they dynamically update their positions to evade predators while maintaining population connectivity. This mechanism facilitates escape from local optima and preserves search diversity. Compared with mainstream counterparts, SSA is characterized by fewer control parameters and a streamlined structural design, which significantly eases practical application and implementation. Benchmarked against unimodal and multimodal test functions, SSA demonstrates superior performance over PSO and Ant Colony Optimization (ACO), enabling efficient identification of global or near-optimal solutions. The mathematical formulation and procedural implementation of SSA are elaborated in the following section.

Step 1: Formulation of the Fitness Function. The fitness function serves as the objective function for structural damage diagnosis and is mathematically defined as follows:

$$\theta_{(x)} = \|Ax - y\|_2 \times (1 + \delta \|x\|_2) \tag{19}$$

In Eq. (19), $\theta_{(x)}$ denotes the fitness value of the candidate solution x, $\|\cdot\|_2$represents the vector 2-norm, and δ refers to the regularization parameter introduced to mitigate numerical ill-posedness. To streamline the computation, δ is empirically set to 0.05 in this study. A lower fitness value indicates a solution closer to the global optimum. Furthermore, Eq. (19) encapsulates a fundamental characteristic of structural damage identification: the solution vector x is inherently sparse, implying that most elements are zero while only a few retain significant non-zero values. This sparsity stems from the physical reality that structural damage in practical engineering is predominantly localized to discrete regions.

Step 2: Initialize the sparrow population. Each sparrow individual is randomly initialized within the predefined bounds as follows:

$$x_{i,j} = v_b + \sigma \times (u_b - v_b) \tag{20}$$

where $x_{i,j}$ refers to the position information of the i-th sparrow at the j-th dimension, namely the j-th variable of the i-th candidate solution, and σ is a random value uniformly generated within [0, 1]. Meanwhile, u_b and v_b separately correspond to the upper and lower bounds of the sparrow position variation range. Conventional optimization algorithms typically adopt the unit hypercube [0, 1] as the default search domain. However, such a fixed interval is inappropriate for objective functions constructed via structural sensitivity equations. This limitation arises because the sensitivity formulation is fundamentally a linear approximation of the static equilibrium equation, which inevitably introduces modeling errors due to linearization. Furthermore, the primary objective of Phase I SSA is damage localization rather than precise quantification. Accordingly, to enhance convergence efficiency, this study defines a constrained narrow-bound search space for Phase I. For instance, the initial search domain is configured as [−0.1, 0.3]. The lower bound of −0.1 accommodates potential negative fluctuations arising from data noise and modeling uncertainties. The upper bound of 0.3 is justified by the fact that incipient structural damage typically manifests as a slight stiffness reduction, usually less than 30% of the intact value. This interval setting encompasses most practical engineering scenarios while effectively accelerating convergence. Notably, this search interval is adaptive; for cases involving extremely slight damage, the bounds can be further contracted based on iterative feedback.

Step 3: Update the positions of producers. The positional update rule for producers is defined as follows:

$$x_{i,j}^{t+1} = \begin{cases} x_{i,j}^{t} \cdot \exp\left(\dfrac{-i}{\gamma \cdot \mu_{\max}}\right), \ R < S_T \\ x_{i,j}^{t} + Q, \ \ R \geq S_T \end{cases} \tag{21}$$

where the superscript t refers to the current iteration number, γ is a stochastic variable defined over the open interval (0, 1], $\mu_{\max}$ denotes the maximum iterative steps, R is a stochastic value distributed in the closed interval [0, 1], S_T corresponds to a preset safety threshold falling within [0.5, 1], and Q represents a random variable obeying the standard normal distribution.

Step 4: Update the positions of scroungers. The positional update rule for scroungers is defined as follows:

$$x_{i,j}^{t+1} = \begin{cases} Q \cdot \exp\left(\dfrac{x_{worst}^{t} - x_{i,j}^{t}}{i^2}\right), \ \ i > \vartheta/2 \\ x_{p}^{t+1} + \left|x_{i,j}^{t} - x_{p}^{t+1}\right| \cdot \upsilon, \ \ otherwise \end{cases} \tag{22}$$

where x_{worst}^{t} refers to the current worst position, ϑ represents the total sparrow population size, υ stands for a random variable ($\upsilon = G^{+}L$, G is a matrix whose elements are randomly assigned a value of 1 or −1, and L is a vector with all elements equal to 1), and the subscript p corresponds to a randomly selected sparrow from the producer group.

Step 5: Update the positions of scouts. The positional update rule for scouts is defined as follows:

$$x_{i,j}^{t+1} = \begin{cases} x_{best}^{t} + \beta \cdot \left| x_{i,j}^{t} - x_{worst}^{t} \right|, & f_i \neq f_g \\ x_{i,j}^{t} + \varsigma \left(\dfrac{\left| x_{i,j}^{t} - x_{worst}^{t} \right|}{(f_i - f_w) + \varepsilon} \right), & f_i = f_g \end{cases} \tag{23}$$

where x_{best}^{t} denotes the present optimal location, β refers to a random variable obeying the standard normal distribution, f_i corresponds to the i-th fitness magnitude, f_g stands for the existing minimum fitness value, f_w represents the current maximum fitness magnitude, ς is a stochastic value distributed over $[-1, 1]$, and ε serves as a tiny constant adopted to avoid zero-division errors.

Step 6: Boundary constraint handling and termination. Following the positional updates, all sparrows are verified to ensure compliance with the predefined search boundaries. Any coordinate violating these limits is reverted to the respective boundary. Subsequently, the fitness values are recalculated based on the adjusted locations. The iteration proceeds until a stopping condition is met, such as hitting the maximum iteration count or fulfilling a custom convergence criterion. This study adopts a convergence criterion based on a 10-iteration sliding window. A check for convergence is performed every 10 iterations. Convergence is declared when both conditions are met for ten consecutive steps: the absolute change in optimal fitness is below 10^{-6}, and the Euclidean norm of the solution change is below 10^{-4}. The loop then stops immediately. In short, it requires the optimal solution and its fitness to remain nearly unchanged for ten straight iterations.

Implementation of Phase I SSA yields preliminary damage coefficients. Elements exhibiting coefficients exceeding the threshold of 0.05 are identified as potential damage regions. This threshold effectively filters out noise-induced fluctuations while highlighting structurally significant damage. It should be noted, however, that this threshold may require further contraction for scenarios involving extremely slight damage assessment. These selected regions will subsequently proceed to Phase II for precise quantitative assessment.

2.3 Damage Quantification via Phase II SSA with Reduced Unknowns

After potential damage locations have been identified, Eq. (15) is condensed by eliminating the column vectors in matrix A and their corresponding coefficients in vector x that pertain to intact structural components. Without loss of generality, assuming that m candidate damaged elements are identified from Phase I, the system of equations is reduced as follows:

$$\overline{A} \cdot \overline{x} = y \tag{24}$$

where $\overline{A}$ denotes a revised matrix reconstructed from A by deleting the vectors linked to intact structural elements, while $\overline{x}$ is a condensed vector generated from x via eliminating the relevant coefficients of undamaged components. Following the exclusion of intact elements, the number of unknown variables in Eq. (24) is significantly reduced. This dimensionality reduction allows Eq. (24) to be resolved again via SSA to acquire more accurate damage quantification. In this secondary execution, the search boundaries are adaptively tuned based on Phase I results to match realistic damage severities, and the iteration count is markedly lowered to boost computational efficiency. Consequently, suspected damaged components are precisely assessed. Elements exhibiting damage parameters above the 0.05 threshold are confirmed as authentic damage, while the rest are classified as intact. For large-scale structures with massive unknowns, this two-stage framework can be iterated to converge to the real solution. It is noted that the sensitivity equation adopted in the above damage diagnosis procedure is the first-order linear approximation of the static response equation. Reference [40] demonstrated that the damage parameters solved by the first-order sensitivity equation are essentially flexibility perturbation parameters, rather than the stiffness damage parameters actually required for damage evaluation. For slight structural damage, flexibility perturbation parameters are numerically close to stiffness damage parameters, and no parameter conversion is required. However, a remarkable discrepancy exists between the two types of parameters under severe damage conditions, and conversion is essential to acquire accurate damage severity values. Reference [40] employed spectral decomposition and matrix inversion techniques to derive the conversion formula between stiffness damage parameters and flexibility perturbation parameters. This formula is also utilized in this study to calibrate the relatively large damage parameters (>0.1) obtained by MS-SSA, so as to rapidly determine the actual damage severity. The specific formula is expressed as follows:

$$\overline{\alpha_i} = \frac{\alpha_i}{1 + \alpha_i} \tag{25}$$

where $\overline{\alpha_i}$ denotes the corrected damage coefficient corresponding to the i-th element. Eq. (25) serves as a direct correction scheme to offset the errors induced by linear approximation in sensitivity analysis. In summary, Fig. 1 illustrates the complete execution flow of the MS-SSA method.

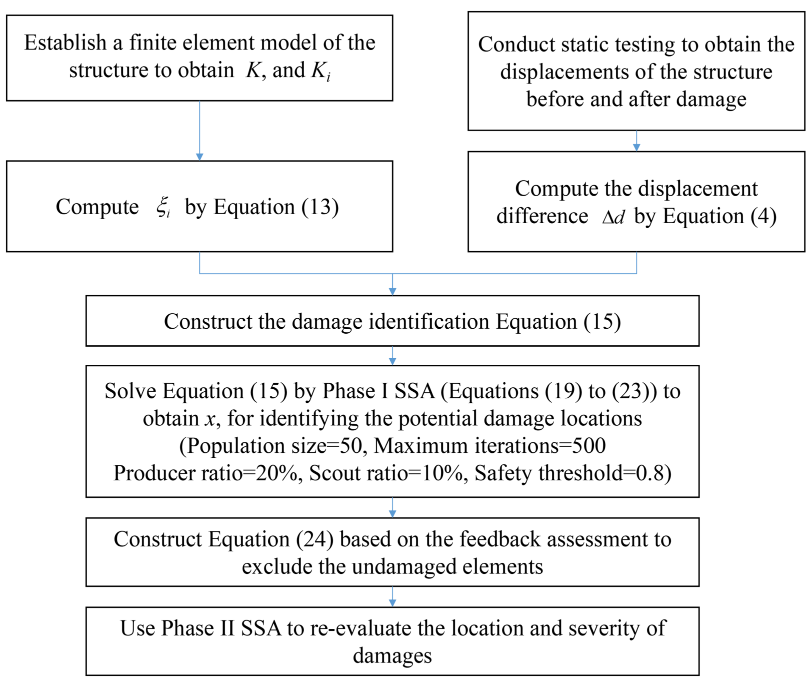

Figure 1: Operational flowchart of MS-SSA.

3 Case Study

The effectiveness of the proposed MS-SSA is validated through a numerical case study followed by an experimental verification. The algorithmic parameters for SSA are configured as follows: a population size of 50, a maximum of 500 iterations, a producer ratio of 20%, a scout ratio of 10%, and a safety threshold (S_T) of 0.8.

3.1 Example 1: A Numerical Lattice Structure

The initial illustration adopted to demonstrate the proposed method is a lattice structure consisting of 58 bars, as depicted in Fig. 2. Within this structure, both the horizontal and vertical bars are 0.5 m in length and have a cross-sectional area of 314 mm^2. The material's elastic modulus is 200 GPa, while its density is 7800 kg/m^3. Vertical loads were applied on nodes 13 and 20, as indicated in Fig. 2, with magnitudes of 150 and 100 kN, respectively. To simulate incomplete measurements in practical scenarios, only the displacement data at nodes 3, 6, 7, 10, 13, 16, 18, 20, 22, 25 and 27 (as shown in Fig. 2) are adopted for damage diagnosis calculations. In addition, 5% noise was added to the static displacement data of the structure to simulate measurement errors in practical scenarios.

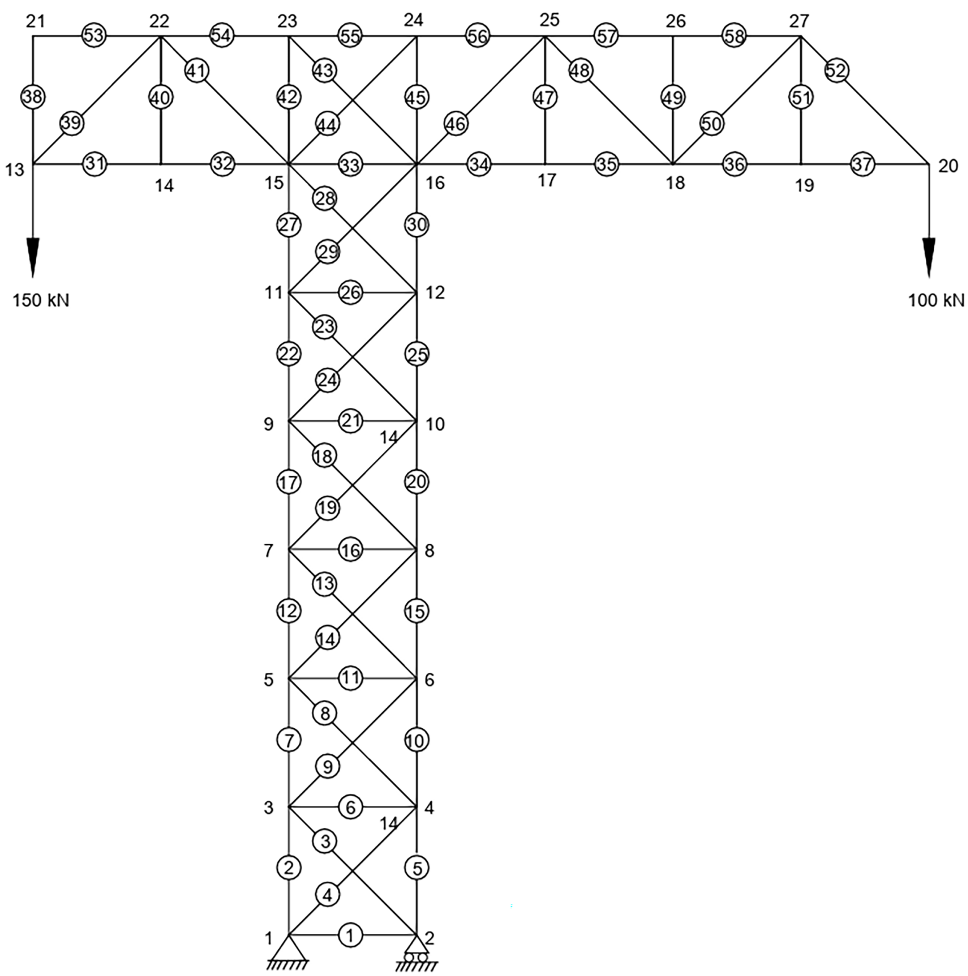

Figure 2: A lattice structure for example 1.

The first damage scenario simulates a 25% loss in the axial stiffness of member 15. Static sensitivity equations were formulated using pre- and post-damage displacement data under the static loading depicted in Fig. 2 for damage assessment. Using noise-free data, Fig. 3 compares the damage parameters identified by three swarm intelligence algorithms: SSA, GWO, and WOA. The initial search interval for SSA was set to [0, 0.4], while GWO and WOA adopted [0, 1]. For comparative purposes, the results of the proposed MS-SSA method are also included in Fig. 3. As observed, SSA, WOA, and MS-SSA correctly identify member 15 as the sole damaged element, whereas GWO erroneously indicates damage in both members 15 and 20. The quantified damage coefficients for member 15 were 0.3220 (SSA), 0.2205 (GWO), 0.3177 (WOA), and 0.2436 (MS-SSA). Compared to the assumed 0.25, these yielded relative errors of 28.8%, 11.8%, 27.1%, and 2.6%, respectively. Notably, the identification error of the proposed method is merely 9%–22% of that associated with existing methods, demonstrating superior accuracy.

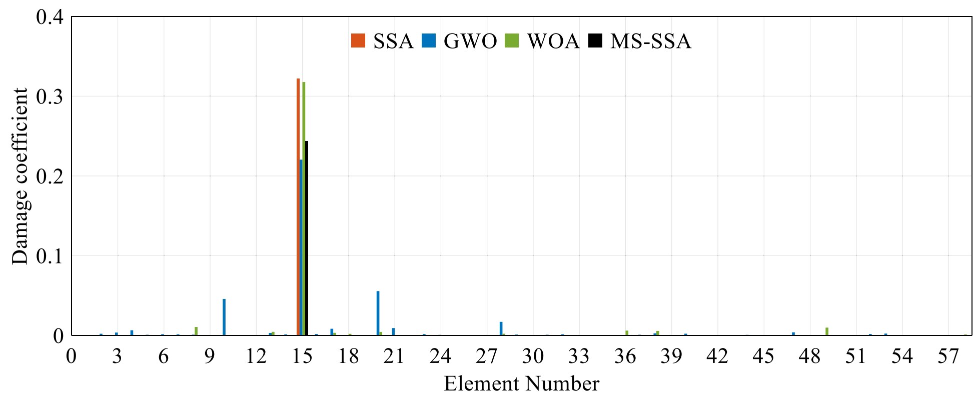

Figure 3: Damage identification results of SSA, GWO, WOA, and MS-SSA for damage in member 15 under noiseless condition.

Using noise-contaminated data, Fig. 4 illustrates the damage parameters obtained via the four methods. Under noise influence, SSA yielded coefficients of 0.0518 and 0.2651 for members 10 and 15, respectively. Both were initially flagged as potential damage sites and were incorporated into Phase II recalculation. Recomputing with SSA resulted in coefficients of 0.0485 and 0.2680. Applying the threshold of 0.05, member 10 was excluded as a false positive. For member 15, the damage coefficient was further calibrated using Eq. (25), resulting in a final value of 0.2114. Thus, MS-SSA successfully identified member 15 as damaged. This confirms that leveraging Phase I feedback for Phase II re-evaluation effectively eliminates spurious identifications and accurately locates actual damage, validating the necessity and rationality of the feedback evaluation step.

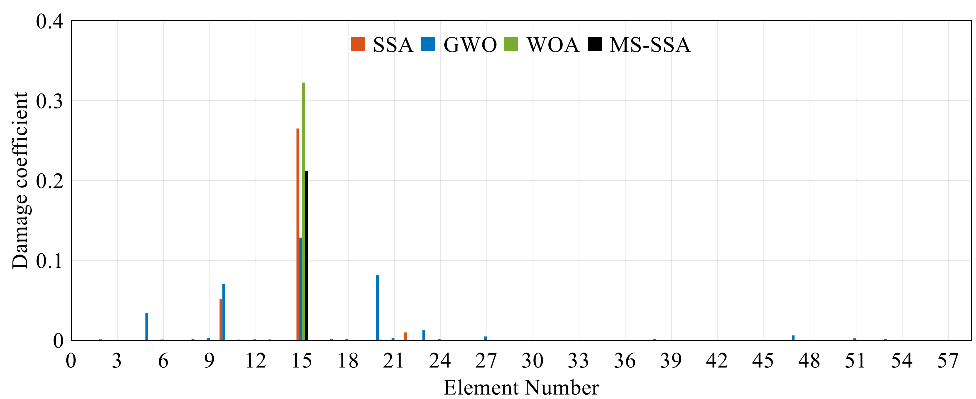

Figure 4: Damage identification results of SSA, GWO, WOA, and MS-SSA for damage in member 15 under 5% noise condition.

The second scenario simulated a 25% and 20% reduction in axial stiffness for members 7 and 46, respectively. Using noise-free data, Fig. 5 compares the damage parameters identified by the four methods. Standard SSA yielded coefficients of 0.2957, 0.2498, and 0.0627 for members 7, 46, and 47, respectively. Consequently, these members were flagged as potential damage sites and subjected to Phase II feedback evaluation. Recomputing with MS-SSA adjusted these values to 0.3219, 0.2499, and 0.0000. Applying the 0.05 threshold excluded member 47 as a false positive. Subsequent calibration via Eq. (25) determined the final coefficients for members 7 and 46 as 0.2435 and 0.1999, corresponding to relative errors of 2.6% and 0.1%. While WOA also identified the correct members with coefficients of 0.3220 and 0.2496, its relative errors (28.8% and 24.8%) were significantly higher than those of MS-SSA. Thus, the proposed method achieves damage assessment results closest to the true values.

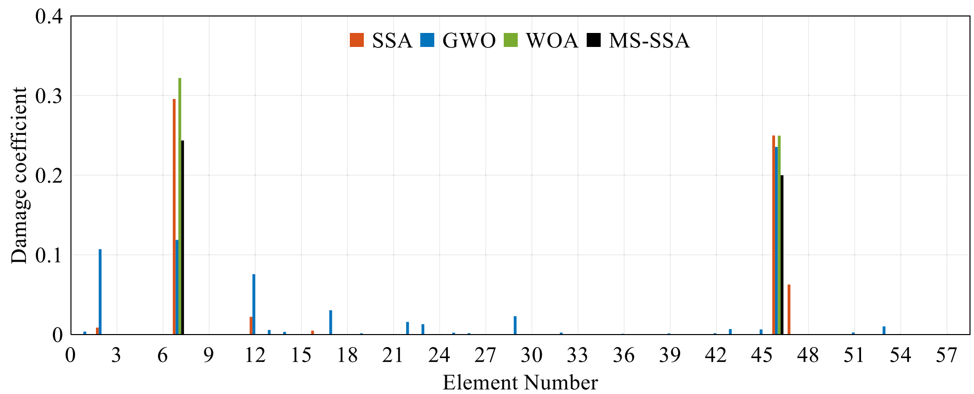

Figure 5: Damage identification results of SSA, GWO, WOA, and MS-SSA for damages in members 7 and 46 under noiseless condition.

As shown in Fig. 6, SSA, GWO, and WOA struggled to accurately pinpoint members 7 and 46 as the sole damaged elements under noisy conditions. Specifically, SSA flagged members 7, 12, and 46 (coefficients > 0.05); GWO identified members 2, 7, 29, and 46; and WOA indicated members 7, 12, 26, and 46. This underscored the necessity of the feedback evaluation. Utilizing the Phase I SSA results, Phase II processing yielded coefficients of 0.3061, 0.0204, and 0.2499 for members 7, 12, and 46, respectively. Member 12 was thereby excluded as a false positive. Final calibration via Eq. (25) determined the coefficients for members 7 and 46 as 0.2344 and 0.1999, corresponding to relative errors of 6.2% and 0.1%. Consequently, the proposed MS-SSA method achieves the highest identification accuracy.

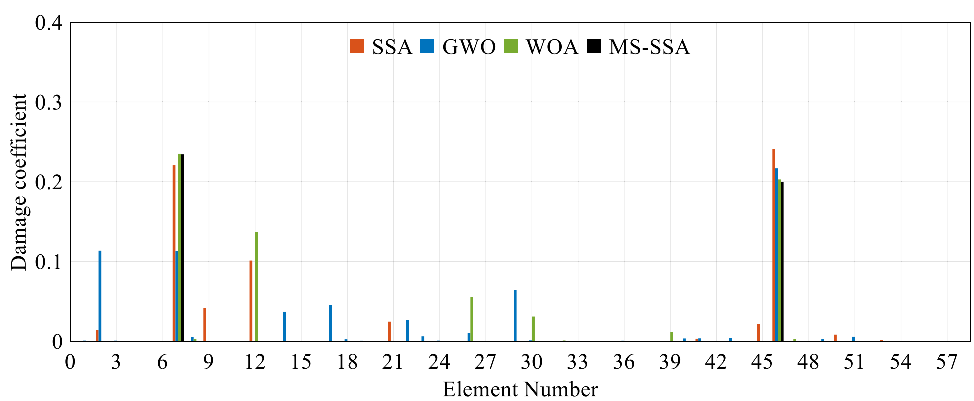

Figure 6: Damage identification results of SSA, GWO, WOA, and MS-SSA for damages in members 7 and 46 under 5% noise condition.

Next, the proposed method was compared with GWO and WOA embedded with L1 regularization. L1 regularization is a strategy for sparse damage diagnosis. Specifically, the 1-norm of x was introduced into the objective functions of GWO and WOA, and their objective function are formulated as follows:

$$\eta_{(x)} = \|Ax - y\|_2 + \lambda \|x\| \tag{26}$$

where $\eta_{(x)}$ denotes the objective function, $\|\cdot\|$ stands for the vector 1-norm, and λ denotes the regularization coefficient used to control the degree of sparsity. A proper value of the regularization coefficient is chosen based on trial computations and engineering experience. In this case, the regularization parameter λ was set to 0.001 by trial calculation. The simulated damage scenario was set as stiffness losses of 5%, 10% and 8% for members 12, 30 and 50, respectively. Another purpose of this scenario is to investigate the performance of various methods under minor damage conditions with the damage severity not exceeding 10%. Since this case is mainly used to compare the performance of various methods under sparse damage, noise-free data were adopted in the subsequent calculations. Fig. 7 shows the identification results of the proposed method, L1-regularized GWO and L1-regularized WOA. As the simulated damage degree in this case is minor, structural members with a damage coefficient exceeding 0.01 were identified as potential damage members. In Fig. 7, the members with damage coefficients identified by GWO exceeding 0.01 were: Member 7 (0.0259), Member 30 (0.1015), and Member 50 (0.0731). The members with damage coefficients identified by WOA exceeding 0.01 were: Member 30 (0.0950) and Member 50 (0.0892). It can be seen from the above results that both GWO and WOA successfully identified Members 30 and 50 as damaged elements, but failed to detect Member 12. This may be attributed to the fact that the damage severity of Member 12 was the smallest. The L1 regularization tends to shrink these tiny coefficients to zero, thereby leading to missing damage detection. As shown in Fig. 7, the members with damage coefficients exceeding 0.01 identified by the Phase I SSA were Member 7 (0.0282), Member 12 (0.0136), Member 24 (0.0387), Member 30 (0.1050), and Member 50 (0.0867). Subsequently, the Phase II SSA was implemented for the above candidate members, yielding the results: Member 7 (0.000), Member 12 (0.0523), Member 24 (0.000), Member 30 (0.1098), and Member 50 (0.0870). As can be seen from the second-stage results, the misjudged Members 7 and 24 in the first stage were eliminated, while Members 12, 30 and 50 were ultimately identified as the actual damaged members. Furthermore, since the damage coefficient of Member 30 exceeded 0.1, Eq. (25) was used for conversion, and its final damage severity was calculated as 0.0989. Compared with the real damage severity values, the identification errors of Member 12, Member 30 and Member 50 were 4.6%, 1.1% and 8.8%, respectively. It has been demonstrated that the multi-stage damage diagnosis strategy can effectively compensate for the drawbacks of single-stage identification, which is prone to damage omission and false identification.

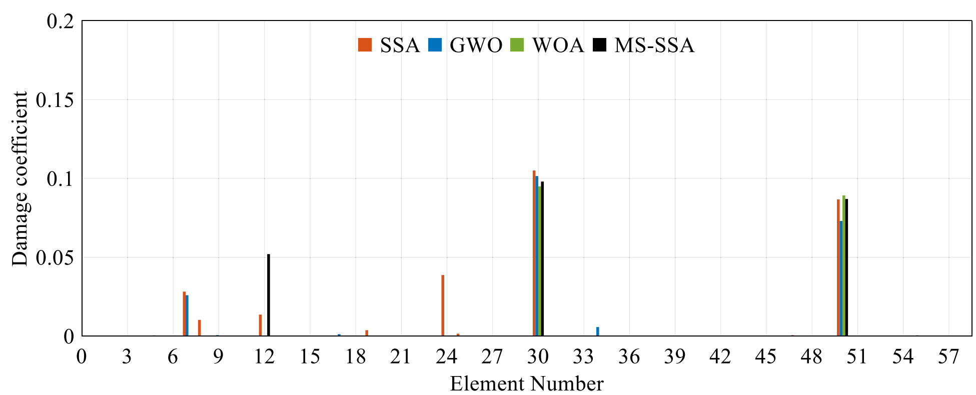

Figure 7: Damage identification results of SSA, GWO, WOA, and MS-SSA for damages in members 12, 30, and 50 under noiseless condition.

It is known that the value of the regularization parameter λ in the fitness function (26) significantly influences the computational results of optimization algorithms assisted by L1 regularization. A larger value of this parameter is intended to yield sparser solutions (i.e., solutions with fewer non-zero elements). While the optimal value of this parameter varies across different engineering problems, experience gained from one problem can often be referenced for others. In practice, it is common to conduct trial calculations by substituting values from several different orders of magnitude into the objective function. In this study, three specific values, λ = 0.01, 0.001, and 0.0001, were selected for testing. The trial results for GWO and WOA are presented in Figs. 8 and 9, respectively. Additionally, the computational results of the SSA employing L1 regularization are provided in Fig. 10 for comparison.

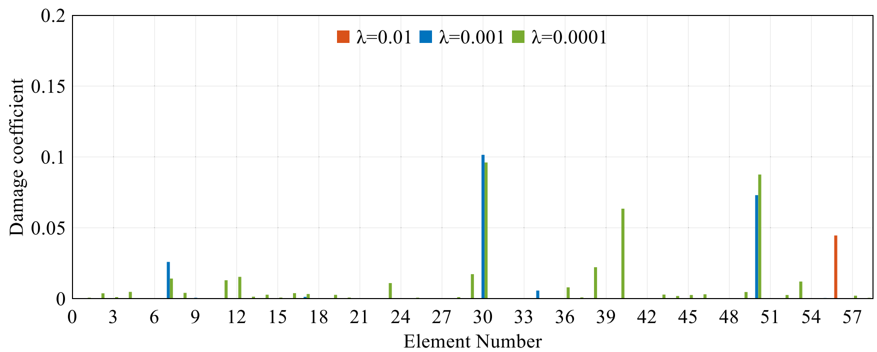

Figure 8: GWO computational results with different regularization coefficients for damaged members 12, 30, and 50.

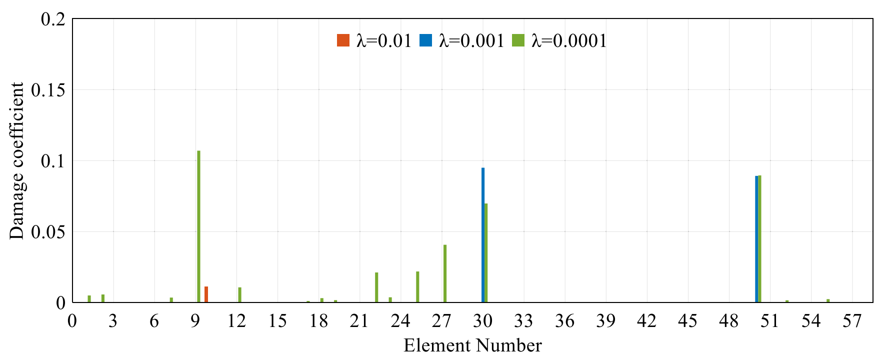

Figure 9: WOA computational results with different regularization coefficients for damaged members 12, 30, and 50.

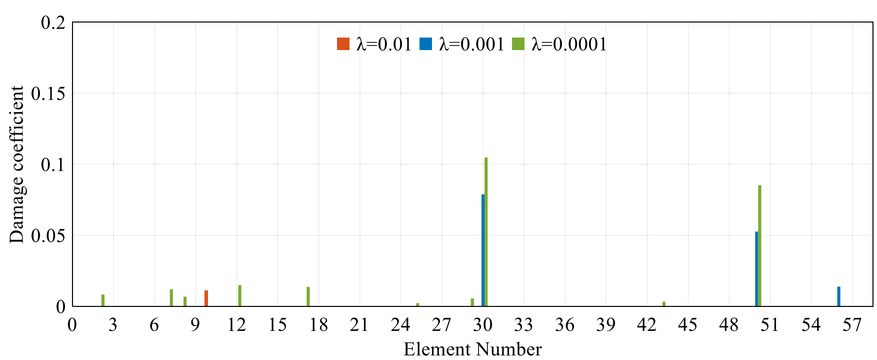

Figure 10: SSA computational results with different regularization coefficients for damaged members 12, 30, and 50.

As shown in Figs. 8–10, as the regularization coefficient λ decreases from 0.01 to 0.001 and further to 0.0001, the number of non-zero elements in the calculation results increases progressively. When λ = 0.0001, the count of non-zero components closely resembles that obtained using L2 regularization. Apart from elements 30 and 50, the three methods employing L1 regularization (GWO, WOA, and SSA) all indicated that numerous other elements may also be damaged. In particular, none of them could clearly identify element 12 as a damaged element. This means that conducting the second-stage precise damage quantification assessment was absolutely necessary. When λ = 0.01 (indicating a relatively large weight for the L1 penalty term), the solution exhibits higher sparsity but was more prone to misidentification and missed detections in scenarios involving multiple damages. Figs. 8–10 show that when the weight of the L1 penalty was too large, only one non-zero element appeared in the calculation results of all three methods, but the results were distorted. In contrast, the results for λ = 0.001 appear to be the most balanced. Figs. 8–10 show that when employing an L1 penalty term with an appropriate weight, all three methods could identify elements with relatively large damage severity (elements 30 and 50), but might miss elements with relatively small damage severity (element 12). Although a more optimal regularization coefficient could be determined through extensive trial calculations, this approach would significantly increase the computational burden and lacked a definitive criterion for optimality (since the true solution is unknown a priori). The process of seeking the optimal regularization parameter through trial calculations to obtain accurate identification results is not as simple and efficient as directly adopting the second-stage precise quantification assessment. Furthermore, even with an optimized regularization parameter, single-stage optimization algorithms still struggle to achieve accurate identification results in multi-damage scenarios. This limitation arises because the large number of unknowns in a single-stage framework inherently restricts the precision of the optimization algorithm. In contrast, the multi-stage identification strategy substantially reduces the number of unknowns in the second stage, enabling the optimization algorithm to ultimately yield highly accurate results; this constitutes the primary innovation of this study.

Additionally, Figs. 8–10 suggest that if the results corresponding to λ = 0.0001 are used to exclude undamaged elements, followed by a re-computation using the optimization algorithm, damage identification results comparable to those of the proposed MS-SSA method could potentially be achieved. This shows that even with L1 regularization, a multi-stage strategy involving initial localization to exclude intact elements before refined quantitative assessment is still necessary and rational.

The performance of the proposed method when a very narrow search interval is adopted in Phase I SSA is discussed in detail below. Without loss of generality, the computational results obtained by various methods using the narrow search interval [0, 0.05] are presented in Fig. 11. As shown in Fig. 11, the narrow search interval [0, 0.05] is utilized by SSA (Phase I), GWO, and WOA, while an adaptive strategy is adopted in Phase II of MS-SSA based on this initial range. Specifically, the search interval is adjusted once every 10 iterations according to the following criteria: (1) if any element of the optimal solution obtained during these 10 iterations exceeds the current upper bound of the search interval, the new upper bound is expanded to 1.2 times the current value; (2) if none of the elements of the optimal solution obtained during these 10 iterations exceed the current upper bound, the new upper bound is set to the midpoint between the current upper bound and the maximum element value of the optimal solution. It can be observed from Fig. 11 that numerous non-zero elements appear in the calculation results of SSA (Phase I), GWO, and WOA when employing the narrow search interval, among which the truly damaged members 12, 30, and 50 are included. Due to the limitation of the search interval, it is impossible for members 30 and 50 to reach their true damage extents of 10% and 8%; however, the damage coefficient values corresponding to these and several other members all attain the upper bound of 0.05 imposed by the search interval. This indicates that adopting a narrow search interval generally does not lead to missed detection of truly damaged members, yet it does result in more members being categorized into the set of potential damaged candidates requiring transfer to the next phase for precise quantitative assessment. The underlying reason for this phenomenon likely lies in the truncation effect of the narrow search interval, wherein the structural response variations caused by members whose damage levels exceed the upper bound of the search interval are forcibly redistributed among other members. However, employing a narrow search interval may offer the benefit of reducing the likelihood of missed detections. Since the narrow interval artificially constrains the contribution of severely damaged members to structural response variations, members with minor damage become easier to identify. However, the search interval in the first stage should not be excessively narrow. An overly narrow interval will result in more elements being classified as potential damage candidates and carried over into the subsequent stage for recalculation, thereby diminishing the effectiveness of the first-stage screening. Obviously, if the number of unknowns remains high in the second stage, the identification results may still lack sufficient accuracy, potentially necessitating a third stage or even further stages of computational refinement. Crucially, Fig. 11 demonstrates that if such a narrow interval is used initially, a second stage of identification becomes indispensable for achieving accurate quantification. Thus, the synergy between narrow-interval initialization and multi-stage feedback is evident: the adaptive search interval applied in the second phase ensures the final accuracy of the results. In Fig. 11, MS-SSA accurately identifies members 12, 30, and 50 as damaged in Phase II, yielding damage coefficients of 0.0523, 0.0989, and 0.087, respectively, which closely match the true values.

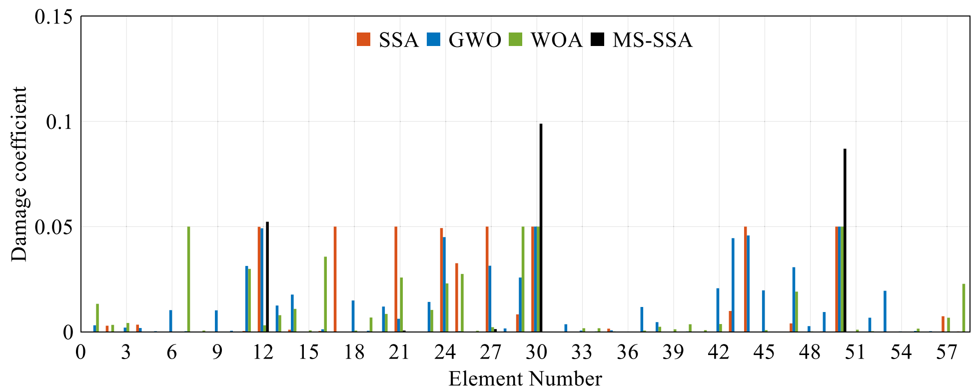

Figure 11: Computational results for damaged members 12, 30, and 50 under a very narrow search interval.

3.2 Example 2: An Experimental Beam Fixed at Both Ends

The experimental data adopted for validating the presented approach originated from the static loading tests of steel beams reported in Reference [41]. Consistent with previous settings, the initial search interval for SSA was set to [0, 0.4], while both GWO and WOA adopted [0, 1]. The basic physical parameters of the beam are as follows: elastic modulus of 193 GPa, material density of 7850 kg/m^3, total length of 0.8 m, section width of 35 mm, and section height of 3 mm. The beam was equally discretized into 16 elements, with each segment being 50 mm long. Fig. 12 illustrates the layout of element labels and node numbers. Four displacement sensors are arranged from left to right at Nodes 6, 8, 10, and 12. As shown in Fig. 12, the notch was located at Element 10. The cutting width was approximately 10 mm (5 mm per side), occupying 28.6% of the total section width of 35 mm. This corresponds to an actual damage degree of approximately 28.6% induced by slot cutting. A 10 N weight was applied at Node 6 to implement static loading. Table 1 summarizes the vertical displacement differences measured at the four sensing points before and after structural damage.

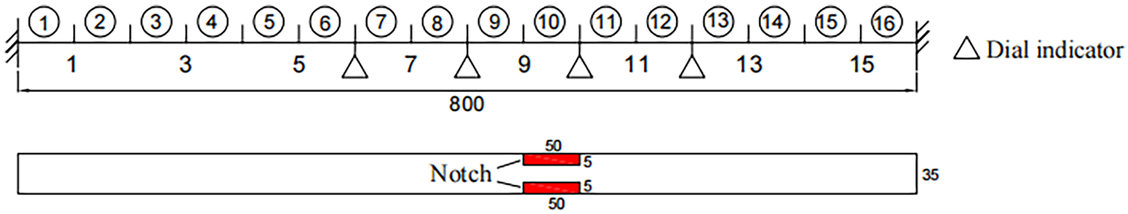

Figure 12: Element and node numbering, and geometric dimensions of example 2 (unit: mm).

Table 1: Measured displacement data of example 2 before and after damage (unit: mm).

Measurement Point Numbering	1	2	3	4
Displacement difference	0.013	0.027	0.030	0.014

Using the data listed in Table 1, Fig. 13 compares the damage parameters of each element identified by solving the sensitivity equations with the four methods. As shown in Fig. 13, although the quantified damage severities differ, all four methods accurately localize the damage at Element 10 of the beam. This consistent performance is primarily attributed to the low dimensionality of the inverse problem in this case. As previously mentioned, the unknowns correspond to the damage parameters of each element to be solved. This beam structure has only 16 elements (i.e., 16 unknowns), which is significantly fewer than the 58 unknowns in the previous numerical example. Generally, fewer unknowns make it easier for various swarm intelligence optimization algorithms to obtain the global optimum. Consequently, all four methods perform well in this case, yielding identical damage localization results due to the low-dimensional nature of the problem. Specifically, the damage coefficients for Element 10 obtained by SSA, GWO, WOA, and MS-SSA were 0.3578, 0.3559, 0.3710, and 0.2707, respectively. Compared to the true damage value of 0.286, their corresponding relative errors were 25.1%, 24.4%, 29.7%, and 5.3%, in turn. The identification error of the proposed method is merely 18%–22% of that of the existing methods. Evidently, MS-SSA delivers the highest accuracy in damage diagnosis.

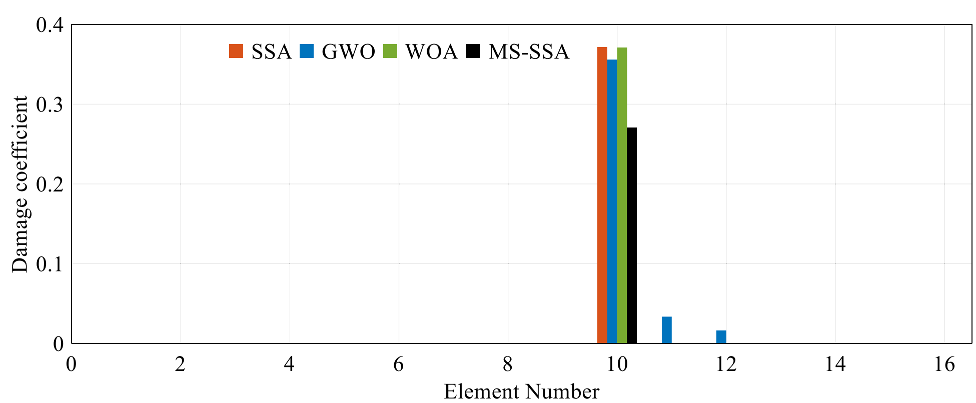

Figure 13: Damage identification results of SSA, GWO, WOA, and MS-SSA for example 2.

4 Results and Discussion

Based on numerical simulation and experimental case study, the main results and findings are as follows:

(1) In simulations, MS-SSA accurately localized single damage and calculated severity more precisely than SSA, WOA, and GWO. For multi-damage cases, only MS-SSA correctly identified locations and severities, while others failed. Experimentally, MS-SSA provided the closest damage estimate to the true value on a steel beam. A 5% noise level was introduced in the numerical simulation to account for measurement errors, as a 5% measurement error is generally considered acceptable in engineering practice. Data noise induces a proliferation of false positives in candidate damage units, a limitation inherent to single-stage identification strategies. In contrast, the multi-stage identification strategy significantly reduces the difficulty of obtaining accurate solutions due to the substantial decrease in the number of unknowns during the second stage. Consequently, the MS-SSA approach enables robust identification performance even under noisy conditions.

(2) The proliferation of unknown parameters poses a formidable challenge to precise damage identification, particularly in multi-damage scenarios. Investigations indicate that single-stage identification relying solely on swarm intelligence optimization algorithms (e.g., SSA, GWO, WOA) is susceptible to false positives and missed detections when addressing structures with high-dimensional unknowns. Consequently, feedback mechanisms and re-evaluation based on initial optimization results are imperative for achieving accurate identification. In this study, the feedback from the first stage was utilized to substantially reduce the number of unknowns for the subsequent stage, followed by a recalculation using SSA. This two-stage paradigm effectively eliminated identification errors and yielded results with superior accuracy, proving especially vital for large-scale engineering structures characterized by extensive unknown variables.

(3) Although L1-regularization-assisted GWO, WOA, and SSA can approximate the true solution by tuning the regularization parameters, they still suffered from a high risk of missed detections, and the search for optimal regularization parameters entails substantial computational costs. In contrast, MS-SSA is more likely to achieve accurate identification results than single-stage methods due to the significant reduction in the number of unknowns during the second stage. This approach can be regarded as replacing the strategy of searching for optimal regularization parameters with a multi-stage identification strategy to achieve accurate damage identification. It is particularly well-suited for damage identification problems in large-scale structures characterized by a vast number of unknown parameters.

(4) Employing a relatively narrow search interval in the first stage generally does not result in missed damage detections; in fact, due to the truncation effect of the narrowed interval, it may even facilitate the identification of relatively minor damage. However, an excessively narrow interval will cause more elements to be classified as potential damage candidates requiring re-evaluation in the second stage, which in turn compromises the identification accuracy of that stage. Based on engineering experience, setting the upper limit of the first-stage search interval within the range of 0.2 to 0.4 is considered reasonable. Furthermore, it is recommended that an adaptive search interval strategy be adopted in the second stage to effectively handle the precise assessment of various damage severities.

5 Conclusion

This study proposes an MS-SSA-based structural damage diagnosis method. The approach utilizes a narrow-interval SSA in the initial stage for preliminary screening of potential damage. Subsequently, the SSA is reused to solve simplified equations with intact elements removed, enabling a more precise damage evaluation. Validation shows this strategy successfully mitigates the missed detections and false positives common in single-stage approaches. It is worth pointing out that the effectiveness of the proposed method relies on the premise that damage can induce observable changes in structural displacements. In other words, if the damage is extremely slight and fails to trigger displacement changes measurable by instruments, the method becomes inapplicable. Future research could focus on developing more effective adaptive search ranges to fully leverage their truncation effect, thereby facilitating the diagnosis of extremely minor damage. Furthermore, investigating multi-round iterative optimization mechanisms holds promise for achieving precise damage identification in large-scale structures characterized by a greater number of unknown variables.

Acknowledgement: Not applicable.

Funding Statement: The authors received no specific funding for this study.

Author Contributions: Methodology, Lijun Yang, and Qiuwei Yang; Investigation, Lijun Yang, and Qiuwei Yang; Software, Lijun Yang, and Qiuwei Yang; Writing, Lijun Yang, and Qiuwei Yang. All authors reviewed and approved the final version of the manuscript.

Availability of Data and Materials: The data used to support the findings of this study are included in this study and are also available from the corresponding author upon request.

Ethics Approval: Not applicable.

Conflicts of Interest: The authors declare no conflicts of interest.

References

1. Bhowmik B, Tripura T, Hazra B, Pakrashi V. First-order eigen-perturbation techniques for real-time damage detection of vibrating systems: theory and applications. Appl Mech Rev. 2019;71(6):060801. doi:10.1115/1.4044287.
2. Avci O, Abdeljaber O, Kiranyaz S, Hussein M, Gabbouj M, Inman DJ. A review of vibration-based damage detection in civil structures: from traditional methods to machine learning and deep learning applications. Mech Syst Signal Process. 2021;147(2):107077. doi:10.1016/j.ymssp.2020.107077.
3. Ruiz DV, de Bragança CSC, Poncetti BL, Bittencourt TN, Futai MM. Vibration-based structural damage detection strategy using FRFs and machine learning classifiers. Structures. 2024;59(2):105753. doi:10.1016/j.istruc.2023.105753.
4. Gandelli E, Rossini G, Mantelli SG, Minelli F. Damage detection of prestressed concrete beams affected by shear and flexure cracks through vibration monitoring. Eng Struct. 2024;304(3):117572. doi:10.1016/j.engstruct.2024.117572.
5. Feng WQ, Mousavi Z, Farhadi M, Bayat M, Ettefagh MM, Varahram S, et al. A hybrid wavelet-deep learning approach for vibration-based damage detection in monopile offshore structures considering soil interaction. J Civ Struct Heal Monit. 2025;15(2):417–44. doi:10.1007/s13349-024-00876-9.
6. Nouri Y, Shahabian F, Shariatmadar H, Entezami A. Structural damage detection in the wooden bridge using the Fourier decomposition, time series modeling and machine learning methods. J Soft Comput Civ Eng. 2024;8(2):83–101. doi:10.22115/SCCE.2023.401971.1669.
7. Teng S, Liu A, Chen B, Wang J, Fu J. Bridge progressive damage detection using unsupervised learning and self-attention mechanism. Eng Struct. 2024;301:117278. doi:10.1016/j.engstruct.2023.117278.
8. Lyu LF, Yuan K, Zhu WD. A novel demodulation method with a reference signal for operational modal analysis and baseline-free damage detection of a beam under random excitation. J Sound Vibr. 2024;571(3):118068. doi:10.1016/j.jsv.2023.118068.
9. Mansouri A, Tiachacht S, Ait-Aider H, Khatir S, Khatir A, Cuong-Le T. A novel optimization-based damage detection in beam systems using advanced algorithms for joint-induced structural vibrations. J Vibr Eng Technolog. 2025;13(7):486. doi:10.1007/s42417-025-02003-4.

10. di Marzo M, Tomassi A, Placidi L. A methodology for structural damage detection adding masses. Res Nondestruct Eval. 2024;35(3):172–96. doi:10.1080/09349847.2024.2336938.
11. Wang Z, Cha YJ. Unsupervised machine and deep learning methods for structural damage detection: a comparative study. Eng Rep. 2025;7(1):e12551. doi:10.1002/eng2.12551.
12. Peng X, Yang QW, Cao HF. Structural damage identification based on mode shape sensitivity and sparrow search algorithm. Structures. 2025;80(6):109999. doi:10.1016/j.istruc.2025.109999.
13. Zar A, Hussain Z, Akbar M, Rabczuk T, Lin Z, Li S, et al. Towards vibration-based damage detection of civil engineering structures: overview, challenges, and future prospects. Int J Mech Mater Des. 2024;20(3):591–662. doi:10.1007/s10999-023-09692-3.
14. Wang X, Hu N, Fukunaga H, Yao ZH. Structural damage identification using static test data and changes in frequencies. Eng Struct. 2001;23(6):610–21. doi:10.1016/S0141-0296(00)00086-9.
15. Peng X, Yang Q. Damage detection in beam-like structures using static shear energy redistribution. Front Struct Civ Eng. 2022;16(12):1552–64. doi:10.1007/s11709-022-0903-4.
16. Abedin M, Caso D, Basalo FJ, Kiani N, Mehrabi AB, Nanni A. Bridge load testing and damage evaluation using model updating method. Eng Struct. 2022;252(4):113648. doi:10.1016/j.engstruct.2021.113648.
17. Cristiani D, Falcetelli F, Yue N, Sbarufatti C, Di Sante R, Zarouchas D, et al. Strain-based delamination prediction in fatigue loaded CFRP coupon specimens by deep learning and static loading data. Compos Part B Eng. 2022;241:110020. doi:10.1016/j.compositesb.2022.110020.
18. Al Thobiani F, Khatir S, Benaissa B, Ghandourah E, Mirjalili S, Abdel Wahab M. A hybrid PSO and Grey Wolf Optimization algorithm for static and dynamic crack identification. Theor Appl Fract Mech. 2022;118(6):103213. doi:10.1016/j.tafmec.2021.103213.
19. Ge L, Koo KY, Wang M, Brownjohn J, Dan D. Bridge damage detection using precise vision-based displacement influence lines and weigh-in-motion devices: experimental validation. Eng Struct. 2023;288(5):116185. doi:10.1016/j.engstruct.2023.116185.
20. Xiao F, Mao Y, Tian G, Chen GS. Partial-model-based damage identification of long-span steel truss bridge based on stiffness separation method. Struct Control Heal Monit. 2024;2024(1):5530300. doi:10.1155/2024/5530300.
21. Kardoulias A, Arailopoulos A, Seventekidis P. From binary to multi-class: neural networks for structural damage classification in bridge monitoring under static and dynamic loading. Dynamics. 2024;4(4):786–803. doi:10.3390/dynamics4040040.
22. Fayyadh MM, Abdul Razak H. Experimental assessment of dynamic and static based stiffness indices for RC structures. Structures. 2022;45:459–74. doi:10.1016/j.istruc.2022.09.051.
23. Naderpour H, Abbasi M, Kontoni DN, Mirrashid M, Ezami N, Savvides AA. Integrating image processing and machine learning for the non-destructive assessment of RC beams damage. Buildings. 2024;14(1):214. doi:10.3390/buildings14010214.
24. Cuevas E, Rodríguez A. Metaheuristic computation with MATLAB. Boca Raton, FL, USA: CRC Press; 2020.
25. Katoch S, Chauhan SS, Kumar V. A review on genetic algorithm: past, present, and future. Multimed Tools Appl. 2021;80(5):8091–126. doi:10.1007/s11042-020-10139-6.
26. Wang D, Tan D, Liu L. Particle swarm optimization algorithm: an overview. Soft Comput. 2018;22(2):387–408. doi:10.1007/s00500-016-2474-6.
27. Yang XS, Deb S. Cuckoo search: recent advances and applications. Neural Comput Appl. 2014;24(1):169–74. doi:10.1007/s00521-013-1367-1.
28. Nadimi-Shahraki MH, Zamani H, Asghari Varzaneh Z, Mirjalili S. A systematic review of the whale optimization algorithm: theoretical foundation, improvements, and hybridizations. Arch Comput Meth Eng. 2023;30(7):4113–59. doi:10.1007/s11831-023-09928-7.
29. Faris H, Aljarah I, Al-Betar MA, Mirjalili S. Grey wolf optimizer: a review of recent variants and applications. Neural Comput Appl. 2018;30(2):413–35. doi:10.1007/s00521-017-3272-5.
30. Rashedi E, Nezamabadi-pour H, Saryazdi S. GSA: a gravitational search algorithm. Inf Sci. 2009;179(13):2232–48. doi:10.1016/j.ins.2009.03.004.

31. Song Y, Cai X, Zhou X, Zhang B, Chen H, Li Y, et al. Dynamic hybrid mechanism-based differential evolution algorithm and its application. Expert Syst Appl. 2023;213(1):118834. doi:10.1016/j.eswa.2022.118834.
32. Xue J, Shen B. A novel swarm intelligence optimization approach: sparrow search algorithm. Syst Sci Control Eng. 2020;8(1):22–34. doi:10.1080/21642583.2019.1708830.
33. Yan S, Liu W, Li X, Yang P, Wu F, Yan Z. Comparative study and improvement analysis of sparrow search algorithm. Wirel Commun Mob Comput. 2022;2022(1):4882521. doi:10.1155/2022/4882521.
34. Gharehchopogh FS, Namazi M, Ebrahimi L, Abdollahzadeh B. Advances in sparrow search algorithm: a comprehensive survey. Arch Comput Meth Eng. 2023;30(1):427–55. doi:10.1007/s11831-022-09804-w.
35. Xue J, Shen B. A survey on sparrow search algorithms and their applications. Int J Syst Sci. 2024;55(4):814–32. doi:10.1080/00207721.2023.2293687.
36. Lv J, Sun W, Wang H, Zhang F. Coordinated approach fusing RCMDE and sparrow search algorithm-based SVM for fault diagnosis of rolling bearings. Sensors. 2021;21(16):5297. doi:10.3390/s21165297.
37. Wan M, Xiao Y, Zhang J. Research on fault diagnosis of rolling bearing based on improved convolutional neural network with sparrow search algorithm. Rev Sci Instrum. 2024;95(4):045111. doi:10.1063/5.0192639.
38. Chang S, Cho M. Dynamic-condensation-based reanalysis by using the Sherman–Morrison–Woodbury formula. AIAA J. 2021;59(3):905–11. doi:10.2514/1.J059738.
39. Yang Q, Peng X. Dynamic modal reanalysis using flexibility disassembly perturbation method. AIAA J. 2024;62(9):3474–90. doi:10.2514/1.J063349.
40. Yang QW. A new damage identification method based on structural flexibility disassembly. J Vibr Control. 2011;17(7):1000–8. doi:10.1177/1077546309360052.
41. Huang X, Peng X, Qin F, Yang Q, Xu B. Damage detection of beam structures using displacement differences and an artificial neural network. Coatings. 2025;15(3):289. doi:10.3390/coatings15030289.